Structure of rhenium surfaces in an oxygen environment

Payam Kaghazchi and Timo Jacob*

Institut für Elektrochemie, Universität Ulm, Albert-Einstein-Allee 47, D-89069 Ulm, Germany

(Received 1 November 2010; revised manuscript received 9 December 2010; published 20 January 2011)

Using density functional theory in conjunction with thermodynamic considerations, we studied different clean and oxygen-covered Re surfaces: low-index Re(0001), Re(10$\bar{1}$0), Re(10$\bar{1}$1), and Re(11$\bar{2}$1) as well as high-index Re(13$\bar{4}$2), all surfaces that were found to be relevant in oxygen-induced surface faceting of rhenium. We found that on more open surfaces oxygen adsorption begins at lower oxygen chemical potentials, which can be correlated to the stronger O–surface interaction. Furthermore, at high-oxygen coverages close-packed Re(0001) becomes significantly more stable than the other Re surfaces that have been investigated. In addition to the stability of surface structures, we also provide quantitative information on the geometries and binding energies, which are of relevance for understanding the properties and catalytic behavior of Re-based catalysts operating under oxygen-rich conditions.

DOI: 10.1103/PhysRevB.83.035417 PACS number(s): 68.03.−g, 71.20.Be, 71.15.Mb

I. INTRODUCTION

Catalysts are often composed of high-surface-area nanoparticles dispersed over a support material. The equilibrium shape of such nanoparticles (in the asymptotic limit given by the Wulff shape[1]) is commonly thought to consist of closely packed surfaces that are likely to have the lowest free energies. For this reason and also for simplicity, these surfaces are mostly taken to model catalysts and are investigated in the presence of the considered reactants (see Refs. 2–5 for related studies on rhenium). However, for some cases it has been shown that even high-index faces might be present on the equilibrium-shaped nanoparticles as well.[6] As atomically rough high-index surfaces, which have higher densities of steps, kinks, and possibly defects, usually show better performance as catalysts than their close-packed counterparts, this has interesting implications for our understanding of the catalysts' properties. Therefore, in order to close the structure gap between real heterogeneous catalysts (e.g., nanoparticles) and surface science models (e.g., low-index surfaces) relevant high-index surfaces have to be considered as well.

Previous studies of transition metal surfaces mainly focused on body-centered-cubic and face-centered-cubic surfaces, while much less attention has been paid to hexagonal-close-packed (hcp) surfaces. In recent years, Re and Re-based catalysts have been used in many important catalytic reactions, such as the selective reduction of NO_x with NH_3, the selective oxidation of methanol, thiophene, as well as hydrodesulfurization, and the ammonia synthesis.[7–12] In addition to their catalytic properties, adsorbate-covered Re surfaces were also used to grow Co nanoclusters, thus providing a basis for synthesizing active model catalysts with high selectivity.[13,14]

Scanning tunneling microscopy images and low-energy electron diffraction (LEED) patterns indicated that dosing a large amount of oxygen (exposure >100 L) on Re(11$\bar{2}$1) at temperatures between 900 and 1000 K leads to the formation of four-sided nanopyramids consisting of (10$\bar{1}$0), (01$\bar{1}$0), and (1×2)-reconstructed (10$\bar{1}$1) and (01$\bar{1}$1) faces.[15] Furthermore, it has been shown that in the presence of nitrogen the planar Re(11$\bar{2}$1) surface becomes completely faceted at 900 K and a pressure of 5×10^{-10} atm. The facets that appeared were characterized as ridgelike structures with faces having (13$\bar{4}$2) and (31$\bar{4}$2) orientations.[15]

Due to its relevance for many reactions (e.g., CO oxidation), here we present theoretical calculations for the adsorption of atomic oxygen on Re(11$\bar{2}$1), Re(10$\bar{1}$0), Re(10$\bar{1}$1), and Re(13$\bar{4}$2) as well as the close-packed Re(0001) surface. On the basis of an extensive set of density functional theory (DFT) calculations for possible adlayer configurations and surface reconstructions we determined the most stable structures of the above-mentioned clean and O-covered Re surfaces. In order to evaluate the preferred surface morphology and composition for specific temperature and pressure conditions, the DFT results were used together with the *ab initio* atomistic thermodynamics approach.[16–19]

The manuscript is organized as follows: In Sec. II, the DFT calculations and the *ab initio* atomistic thermodynamics method as used in the present work are briefly described. Our results for different clean and O-covered Re surfaces are discussed in Sec. III, and in Sec. III C these results are then used to construct the stability phase diagrams for different O/Re surfaces. Finally, conclusions and outlook are given in Sec. IV.

II. METHOD

The macroscopic behavior of materials is mostly determined by the interactions at the microscopic level. Therefore, in order to investigate the surface structures and compositions, we first employed DFT to obtain information on the adsorption and binding energies (microscopic scale), which were then used in conjunction with statistical mechanics to connect to the macroscopic behavior. In particular, the *ab initio* atomistic thermodynamics approach had been used to evaluate (p,T)-dependent surface free energies.[16–19]

A. DFT calculations

All first-principles calculations were performed with the Cambridge Serial Total Energy Package (CASTEP),[20] a periodic plane-wave-based DFT program. We have used Vanderbilt-type ultrasoft pseudopotentials[21] to replace the core electrons, and the valence space has been expanded in plane waves. Throughout this work, exchange-correlation energies were

evaluated with the Perdew-Burke-Ernzerhof (PBE)[22] form of the generalized-gradient approximation (GGA). All slab geometries were constructed on the basis of the calculated lattice constants of $a_0 = 2.78$ Å and $c_0 = 4.48$ Å.

After extensive convergence tests,[23,24] we established calculational parameters for the basis-set energy cutoff, the number of k points, and slab and vacuum thickness and evaluated the accuracy of the pseudopotential. On the basis of these studies we used a plane-wave basis set with an energy cutoff of 380 eV for all surfaces. The Brillouin zones of the corresponding (1×1) surface unit cells of Re(0001), Re(10$\bar{1}$0), Re(10$\bar{1}$1), Re(11$\bar{2}$1), and Re(13$\bar{4}$2) were sampled with (8×8), (5×8), (4×8), (4×4), and (3×3) Monkhorst-Pack k-point meshes, respectively. These surfaces were represented by 5-layer, 11-layer, 14-layer, 19-layer, and 30-layer slabs, respectively, where the bottom 2, 4, 4, 4, and 14 layers were fixed at the calculated bulk structure, and the geometry of the remaining layers was fully optimized (up to <0.03 eV/Å). In order to avoid interactions between period images, slabs were separated by a vacuum of at least 13 Å.

B. The *ab initio* atomistic thermodynamics approach

Here we briefly discuss the *ab initio* atomistic thermodynamics approach,[16–19] as it was used in the present work to evaluate the stability of O/Re systems.

The most stable structure of a surface (here Re) in thermodynamic equilibrium with a gas atmosphere (here O_2) is the one that has the lowest surface free energy expressed as[19]

$$\gamma(T,\{p_i\},\{N_i\}) = \frac{1}{A}[G_{\text{surf}}(T,\{p_i\},\{N_i\}) - \sum_i N_i \mu_i(T,p_i)], \; i = \text{Re,O}. \quad (1)$$

Here G_{surf} is the Gibbs free energy of the slab with area A, consisting of N_i atoms of the ith species, whose reservoir is characterized by the chemical potential $\mu_i(T,p_i)$ and the partial pressure p_i, and T is the temperature. Assuming the temperature and pressure dependence of all solid phases to be small,[25,26] we can rewrite Eq. (1) as

$$\gamma\left(T,p_{O_2},N_{\text{Re}},N_{\text{O}}\right) = \frac{1}{A}\left[G_{\text{surf}}(T,p_{O_2},N_{\text{Re}},N_{\text{O}}) - N_{\text{Re}}\mu_{\text{Re}}^{\text{bulk}} - N_{\text{O}}\mu_{\text{O}}(T,p_{O_2})\right]. \quad (2)$$

The chemical potential of the oxygen gas phase can be described by the ideal gas law, which then enables us to relate μ_{O} to specific temperatures and pressures:

$$\mu_{\text{O}}^{\text{gas}}(T,p_{O_2}) = \frac{1}{2}\left[E_{O_2}^{\text{tot}} + \bar{\mu}_{O_2}(T,p^0) + k_{\text{B}}T\ln\left(\frac{p_{O_2}}{p^0}\right)\right], \quad (3)$$

where $E_{O_2}^{\text{tot}}$ is the calculated total energy of an isolated O_2 molecule and $\bar{\mu}_{O_2}(T,p^0)$ is the standard chemical potential at temperature T, which includes all the contributions from vibrations and rotations of the molecule and the ideal gas entropy at 1 atm. Although the standard chemical potentials can be calculated from first principles, for the phase diagrams that will be discussed in Sec. III C, we used the corresponding $\bar{\mu}_{O_2}(T,p^0)$ values from the JANAF thermodynamic tables.[27]

III. RESULTS AND DISCUSSION

A. Clean surfaces

The hcp structures such as adopted by metallic rhenium involve two interpenetrating Bravais lattices. In this kind of material we have two distinguishable types of atoms. Therefore, in almost all cases, cleaving the hcp crystal along a particular direction creates two different surface structures, depending on which kind of atoms are exposed. Using the four-index notation we label two different possible terminations of Re surfaces by (*ijkl*)A and (*ijkl*)B.

The stability of different clean Re surfaces (see Fig. 1) are compared through the surface free energy defined by Eq. (2) with $N_{\text{O}} = 0$.

The LEED measurements on Re(10$\bar{1}$0) show an unreconstructed (1×1) structure for the clean surface[28,29] and a (1×3) periodicity after oxygen adsorption.[5,30] Since the experimentally observed (1×3) periodicity for O/Re(10$\bar{1}$0) could also be due to a corresponding missing-row (MR) reconstruction of the surface, in addition to the unreconstructed surface, the three possible reconstructed Re(10$\bar{1}$0)A-(1×3) surfaces shown in Figs. 1(b4)–1(b6) were considered along with the (1×2)-reconstructed Re(10$\bar{1}$0)A surface (see Fig. 1(b3)). The latter type of reconstruction has been observed on another low-index surface of Re, namely the (10$\bar{1}$1) orientation: Oxygen adsorption on Re(11$\bar{2}$1) leads to the formation of four-sided nanopyramids consisting of Re(10$\bar{1}$0), Re(01$\bar{1}$0), Re(10$\bar{1}$1)-(1×2), and Re(01$\bar{1}$1)-(1×2) faces.[13] To determine whether clean Re(10$\bar{1}$1) reconstructs, we considered Re(10$\bar{1}$1)-(1×2) in addition to two different configurations of Re(10$\bar{1}$1)-(1×1) [see Figs. 1(c1)–1(c3)].

The calculated surface free energies for the clean Re surfaces are listed in Table I. While all energies were evaluated by means of DFT-PBE, the most stable structures were additionally calculated using the LDA (local density approximation) functional. Although surface free energies of clean surfaces calculated with LDA are usually expected to be in better agreement with experiment compared to the PBE results,[31] this is different for surface adsorptions. Here Hammer *et al.*[32] have shown that including gradient corrections (GGA-PBE) reduces the LDA overbinding of the chemisorbed atoms on metals. Therefore, in the present work we use the PBE functional to calculate oxygen adsorption energies and free energies of oxygen-covered surfaces. In this context it is interesting that for the clean Re surfaces studied in this work the LDA surface free energies are larger than the corresponding PBE values by almost identical amounts (between 31 and 35 meV/Å^2). Nevertheless, both DFT-PBE and DFT-LDA calculations suggest the following order of stability: $\gamma_{0001} < \gamma_{10\bar{1}0} < \gamma_{10\bar{1}1} < \gamma_{13\bar{4}2} < \gamma_{11\bar{2}1}$. The surface free energy of (13$\bar{4}$2) is slightly lower than that obtained for (11$\bar{2}$1), though the former surface is much more open and would thus be expected to be less stable (i.e., higher surface free energy). The observed contrary behavior is probably due to the unique structure of Re(13$\bar{4}$2), which can be viewed as a vicinal (01$\bar{1}$1) surface with kinked steps and (01$\bar{1}$1) terraces that are more close-packed than (11$\bar{2}$1).[13] This picture is also supported by our DFT results (see Table I), which show that the surface free energy of Re(13$\bar{4}$2) is similar to that of Re(01$\bar{1}$1) terraces.

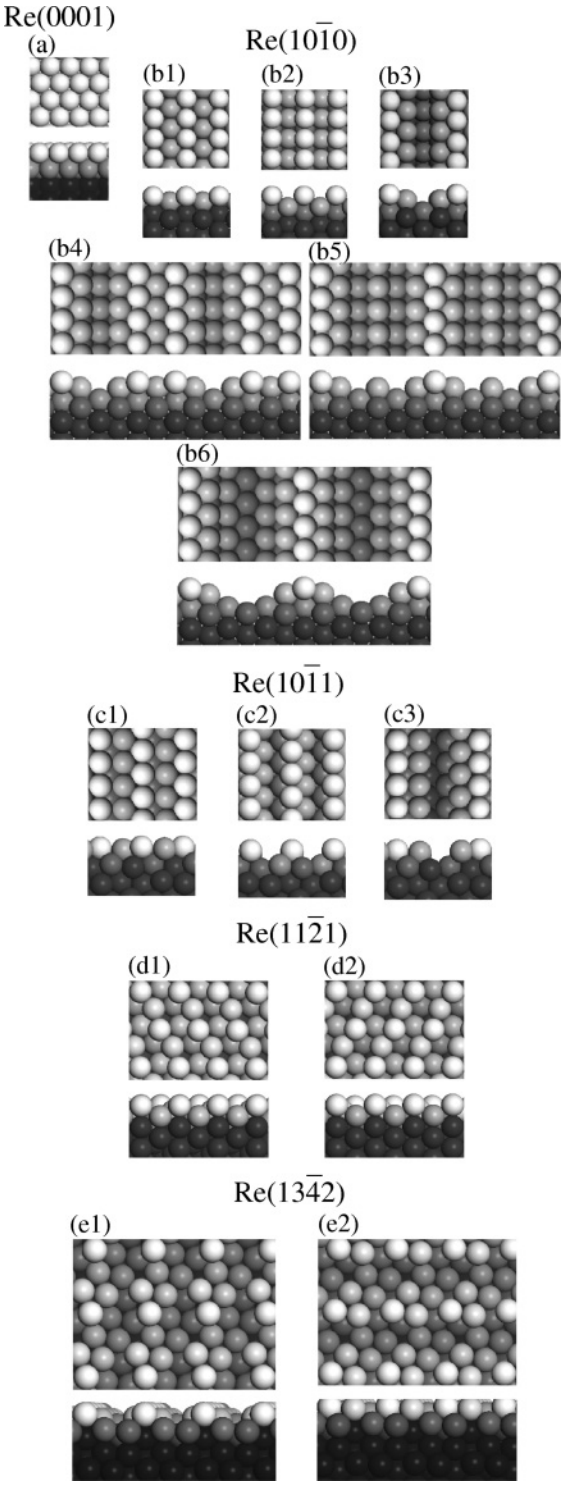

FIG. 1. Top and side views of (a) Re(0001), (b1) Re(10$\bar{1}$0)A-(1 × 1), (b2) Re(10$\bar{1}$0)B-(1 × 1), (b3) Re(10$\bar{1}$0)A-(1 × 2), (b4) Re(10$\bar{1}$0)A-(1 × 3) single-MR, (b5) Re(10$\bar{1}$0)A-(1 × 3) double-MR, (b6) Re(10$\bar{1}$0)A-(1 × 3) triple-MR, (c1) Re(10$\bar{1}$1)A-(1 × 1), (c2) Re(10$\bar{1}$1)B-(1 × 1), (c3) Re(10$\bar{1}$1)A-(1 × 2), (d1) Re(11$\bar{2}$1)A, (d2) Re(11$\bar{2}$1)B, (e1) Re(13$\bar{4}$2)A, and (e2) Re(13$\bar{4}$2)B surfaces. The layers become darker with increasing depth.

We find that, among the studied Re(10$\bar{1}$0) surfaces, unreconstructed Re(10$\bar{1}$0)A is most stable [see Fig. 1(b1)]. The alternative configuration Re(10$\bar{1}$0)B, which is less closely packed, is less stable by 68 meV/Å^2. This is in agreement with experimental studies by Davis *et al.*[28] Table I also indicates that clean unreconstructed Re(10$\bar{1}$0)A-(1 × 1) is considerably more stable than all reconstructed surfaces. Thus, in line with the experimental results for Re(10$\bar{1}$0)[28,29] and other 3*d* and 4*d* hcp(10$\bar{1}$0) metal surfaces,[33,34] our calculations indicate no preference for such kind of reconstruction of clean Re(10$\bar{1}$0).

TABLE I. Surface free energies (in meV/Å^2) for Re surfaces obtained using the PBE and LDA functionals. The corresponding structures are shown in Fig. 1.

Structure	PBE	LDA
Re(0001)	171	202
Re(10$\bar{1}$0)A	183	215
Re(10$\bar{1}$0)B	251	···
Re(10$\bar{1}$0)A-(1 × 2)	236	···
Re(10$\bar{1}$0)A-(1 × 3) single MR	216	···
Re(10$\bar{1}$0)A-(1 × 3) double MR	240	···
Re(10$\bar{1}$0)A-(1 × 3) triple MR	221	···
Re(10$\bar{1}$1)I	209	242
Re(10$\bar{1}$1)II	243	···
Re(10$\bar{1}$1)III-(1 × 2)	226	···
Re(11$\bar{2}$1)A	220	255
Re(11$\bar{2}$1)B	220	···
Re(13$\bar{4}$2)A	217	251
Re(13$\bar{4}$2)B	217	···

The surface corrugation of Re(10$\bar{1}$1)A-(1 × 1) is smaller than that of Re(10$\bar{1}$1)B-(1 × 1). Therefore, the surface free energy of the former (213 meV/Å^2) turned out to be 30 meV/Å^2 lower. DFT-PBE calculations yield a surface free energy of 226 meV/Å^2 for the (1 × 2)-MR structure, which is 13 meV/Å^2 larger than the value obtained for the corresponding unreconstructed surface.

As can be seen from Figs. 1(d1) and 1(d2), Re(11$\bar{2}$1)A and Re(11$\bar{2}$1)B are mirror symmetric to each other, and therefore, we find the same surface free energy for these surfaces. Although this is not the case for different surface terminations of (13$\bar{4}$2) (A and B), they turned out to also have the same stability.

On the basis of the above-mentioned results we can conclude that for the studied Re-surfaces the clean (*ijkl*)A structures have either higher or similar stabilities compared to their corresponding clean (*ijkl*)B surfaces. Thus, hereafter, we concentrate on (*ijkl*)A surfaces only and refer to them as (*ijkl*).

B. Oxygen adsorption on Re surfaces

After the clean surfaces, the adsorption of atomic oxygen with different overlayers and coverages was studied to gain insights into the stability of adsorbate structures as function of coverage. In our calculations, coverages Θ are given in geometrical monolayers (GML), which are defined as the number of adsorbate atoms per (1 × 1) unit cell of the substrate, thus varying with surface orientation. For reconstructed surfaces, we also define Θ as the number of adsorbate atoms per (1 × 1) unit cell of the corresponding unreconstructed surface.

On Re(0001), Re(10$\bar{1}$0), Re(10$\bar{1}$1), and Re(11$\bar{2}$1) surfaces, coverages smaller than 1.0 GML were studied, while on Re(13$\bar{4}$2), which has a rather extended and open surface unit

cell, we only investigated coverages larger than 1.0 GML. Therefore, on Re(13$\bar{4}$2) interactions between adsorbates in adjacent unit cells are already expected to be negligible at 1.0 GML. For systems with more than one adsorbate per (1×1) unit cell, several combinations of adsorption sites have been studied. These configurations have been chosen by considering the calculated energies for lower coverages and then trying to find the lowest destabilization due to adsorbate–adsorbate repulsion at higher coverages.

The most favorable structure at a given coverage of oxygen on a surface is the one with the largest average binding energy as defined by

$$E_{\text{bind}} = -\frac{1}{N_{\text{O}}}\left[E_{\text{O/slab}} - E_{\text{slab}} - N_{\text{O}}\left(\frac{1}{2}E_{\text{O}_2}^{\text{tot}}\right)\right], \quad (4)$$

where N_{O} is the number of oxygen atoms in the considered unit cell and $E_{\text{O/slab}}$, E_{slab}, and $E_{\text{O}_2}^{\text{tot}}$ are the total energies of the oxygen-covered Re surface slab, the clean Re surface slab, and the isolated oxygen molecule, respectively. According to this definition a positive number indicates that the dissociative adsorption of oxygen from gas-phase O_2 is exothermic. The binding energies of oxygen for the most stable structures are listed in Table II.

Furthermore, we define $\bar{E}_{\text{bind}}$ as the averaged binding energy of combinations of single-adsorbate systems:

$$\bar{E}_{\text{bind}} = \frac{1}{N_{\text{O}}}\sum_{i=1}^{N_{\text{O}}} E_{\text{bind}}^{i} \quad (\Theta = 1\,\text{GML}). \quad (5)$$

From this value we can roughly estimate the adsorbate–adsorbate interaction energy by evaluating the difference $\bar{E}_{\text{bind}} - E_{\text{bind}}$. Thus, on rather open surfaces, we expect deviations between both energies for $\Theta \geqslant 2$ GML.

1. O/Re(0001)

LEED studies by Zehner *et al.*[5] showed half-order beams in the (10$\bar{1}$0) and (11$\bar{2}$0) azimuths for exposures of 5×10^{-8} Torr · min on Re(0001) at temperatures between ∼888 and ∼1193 K. They proposed that possible structures producing such a diffraction pattern are either the (2×2)-1O overlayer or the superposition of three (2×1)-1O overlayers rotated by 120° to each other (following the threefold surface symmetry). Moreover, a (1×1) structure was observed at exposures of 2×10^{-6} Torr · min at the above-mentioned temperature range. Using auger-electron spectroscopy and LEED, Ducros *et al.*[4] observed the previously reported (2×2) periodicity by heating Re(0001) to around 500 K. Since the coverage associated with this structure was measured to be one-half of the maximum coverage [0.5 PML (physical monolayer)], they proposed the superposition of three (2×1)-1O overlayers and excluded the possibility of (2×2)-1O formation suggested by Zehner *et al.*[5] Furthermore, they could not observe the (1×1) structure as reported by Zehner *et al.*[5] after high exposures of oxygen, but rather observed the (2×2) structure at all exposures and temperatures up to 1400 K.

Motivated by these deviating results, we performed calculations of the following oxygen coverages on Re(0001): $\Theta = 0.25, 0.50$, and 1.00 GML. Since for $\Theta = 0.25$ GML the separation between adsorbates (∼5.6 Å) is rather large, we expect very small O–O interactions at this coverage. In order to determine the preferred binding site we considered one adsorbate per (2×2) unit cell ($\Theta = 0.25$ GML) and calculated the binding energy at all possible on-surface sites shown in Fig. 2(a). It was found that oxygen binds most strongly at the threefold H2 site, where a Re atom is in the layer beneath

TABLE II. Binding energies (referenced to 1/2 O_2) and sites for oxygen on Re surfaces at different coverages. Only the most stable structure for each coverage is listed.

Structure	Coverage (GML)	Binding site	E_{bind} (eV)
Re(0001)	0.25	H2	3.48
	0.50	H2	3.55
	1.00	H2	3.38
Re(10$\bar{1}$0)-(1×1)	0.25	H1	3.76
	0.33	H1	3.66
	0.50	H1	3.79
	0.66	H1	3.61
	1.00	H1	3.60
	1.33	H1	3.28
	1.50	H1	3.17
	1.66	H1	3.01
	2.00	H1	2.76
Re(10$\bar{1}$0)-(1×2)-MR	0.50	H1	3.89
	1.00	H1/H1	3.58
	2.00	H1/H1/H3/H3′	2.98
Re(10$\bar{1}$0)-(1×3)-MR	0.33	H1	3.84
	0.66	H1/H1′	3.78
	1.00	H1/B3/H1′	3.53
	1.33	H1/B3/H3/H1′	3.36
	1.66	H2/T3/H4/H2′/H4′	3.21
	2.00	H1/H3/H5/H1′/H3′/H4′	3.04
Re(10$\bar{1}$1)-(1×1)	0.25	H1	3.79
Fig. 6(c1)	0.50	H1	3.80
Fig. 6(c2)	0.50	H2	3.65
Fig. 6(d1)	1.00	B2	3.55
Fig. 6(d2)	1.00	H2	3.53
Fig. 6(d3)	1.00	H1	3.51
Fig. 6(e1)	2.00	H2/B2	3.12
Fig. 6(e2)	2.00	H1/B2	3.10
Re(10$\bar{1}$1)-(1×2)-MR	0.25	H2	3.90
	0.50	H2	3.87
	1.00	H2/B4	3.60
	2.00	H2/H3/H4/H5	3.19
Re(11$\bar{2}$1)			
Fig. 9(b1)	0.50	B5	3.82
Fig. 9(b2)	0.50	B5	3.81
	1.00	B5	3.85
	2.00	B1/H	3.48
	3.00	B1/B3/H2	2.98
Re(13$\bar{4}$2)	1.00	H1	4.03
	2.00	H1/B7	3.78
Fig. 11(d1)	3.00	H1/B7/B6	3.67
Fig. 11(d2)	3.00	H1/B7/H9	3.63
Fig. 11(e1)	4.00	H1/B7/B6/H7	3.55
Fig. 11(e2)	4.00	H1/H6/B6/H7	3.54
	5.00	H1/B7/B6/H7/H11	3.38
	6.00	H1/B7/B6/H7/H11/H4	3.15

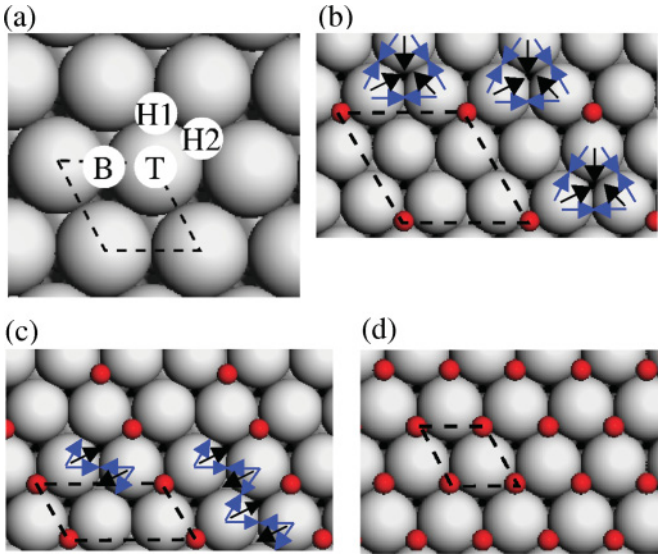

FIG. 2. (Color online) Top views of Re(0001) showing (a) all binding sites at which O adsorption has been studied as well as the most stable structures of oxygen-covered Re(0001) with different overlayers and coverages: (b) (2 × 2)-1O at 0.25 GML, (c) (2 × 1)-1O at 0.50 GML, and (d) (1 × 1)-1O at 1.00 GML. The blue (gray) arrows show row-paired atoms, while the black arrows show the resulting movements of atoms due to row pairing.

it. This result is in line with the experimental and theoretical findings for O/Ru(0001).[35,36]

The calculated binding energy of 3.48 eV for O at H2 sites is 0.57 eV stronger than adsorption at the second favorable site (H1 site). The binding energy difference remains almost unchanged in the coverage range of 0.25 GML $\leqslant \Theta \leqslant$ 1.00 GML (see Fig. 3).

At $\Theta = 0.50$ GML, we find the experimentally proposed (2 × 1)-1O overlayer where O occupies H2 sites [see Fig. 2(c)]. This structure leads to a binding energy of 3.55 eV. Analyzing the geometries of clean and O-covered Re(0001) surfaces shows the existence of *row pairing* (RP) of Re atoms induced by O adsorption for $\Theta = 0.25$ and 0.50 GML. This behavior has also been reported on Re(10$\bar{1}$0), Ir(110), and Ir(311) surfaces, and it seems to be a more general phenomenon for transition metals.[23] As a consequence of the strong interaction

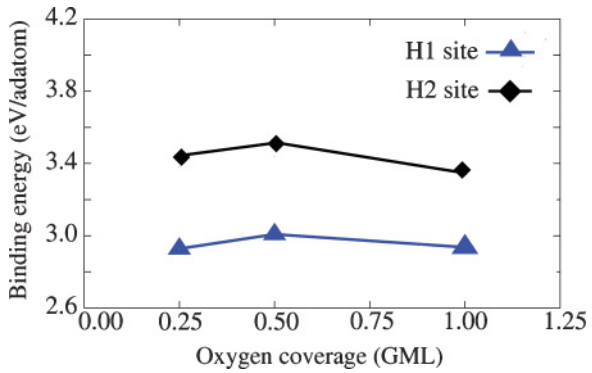

FIG. 3. (Color online) Binding energy (referenced to 1/2 O_2) as a function of oxygen coverage on Re(0001) for adsorption at H1 and H2 sites.

between oxygen and the surface, Re atoms to which the adatom binds are displaced (by 0.08 Å at $\Theta = 0.25$ GML and 0.09 Å at $\Theta = 0.50$ GML) from their bulk-truncated positions, finally causing the binding energy to increase.

As can be seen in Fig. 2, the number of row-paired (substrate) atoms at 0.25 GML is 3/2 times more than at 0.50 GML, and thus, higher energy gain is expected for the former coverage. To estimate the contribution of this energy gain (due to the row pairing) to the overall binding energy, we evaluated the difference between the oxygen binding energies before and after row pairing. We found that the energy gain (per O adatom) due to this effect is 0.11 and 0.08 eV per oxygen atom for coverages of 0.25 and 0.50 GML, respectively.

Despite the smaller energy gain due to row pairing and destabilization introduced by O–O repulsion for 0.50 GML, the calculated binding energy for this coverage is 0.07 eV stronger than that for 0.25 GML. This is in agreement with experimental studies,[4] evidencing formation of the (2 × 2)-2O adlayer ($\Theta = 0.50$ GML) but not the (2 × 2)-1O structure ($\Theta = 0.25$ GML).

2. O/Re(10$\bar{1}$0)

Annealing O-covered Re(11$\bar{2}$1) generates nanoscale pyramids exposing (10$\bar{1}$0) and (10$\bar{1}$1) faces. In a previous study we already investigated the details of O adsorption on Re(10$\bar{1}$0).[24] Therefore, here we only give a brief summary of the main results. To determine the most stable structures for different coverages of O on this surface, we considered a variety of adsorption sites and their combinations on the unreconstructed Re(10$\bar{1}$0)-(1 × 1) as well as MR-reconstructed Re(10$\bar{1}$0)-(1 × 2) and (1 × 3) surfaces (see Fig. 4).

The calculated binding energy of oxygen (in the most favorable configuration) as a function of coverage is summarized in Fig. 5. Again, due to row pairing of Re atoms for coverages lower than 1.00 GML on the unreconstructed surface the binding energy increases by ∼0.1 eV per oxygen atom at both $\Theta = 0.25$ and 0.50 GML (see Fig. 5). The adsorption energy of O is found to be higher on the reconstructed surfaces than on the unreconstructed surface for most of the considered coverages except for 1.00 GML. The stabilization resulting from the MR reconstruction is more significant at higher coverages, showing that additional O atoms prefer sites in the troughs of the missing rows. Therefore, at the highest studied coverage (2.00 GML) the strongest binding energy of O is found on the triple-MR structure, which has the deepest trough among the studied systems (see Ref. 24 for more details).

3. O/Re(10$\bar{1}$1)

From LEED experiments, Wang *et al.* proposed that the (10$\bar{1}$1) faces, which are formed in addition to the (10$\bar{1}$0) faces on O-induced surface facets on Re(11$\bar{2}$1), are reconstructed and have a (1 × 2) missing-row structure.[15]

Here we will discuss our results for oxygen adsorption on unreconstructed Re(10$\bar{1}$1)-(1 × 1) and MR-reconstructed Re(10$\bar{1}$1)-(1 × 2) for a variety of coverages: $\Theta = 0.25$, 0.50, 1.00, and 2.00 GML. To determine the preferred binding sites for oxygen on these surfaces, we studied all sites indicated in Figs. 6(a) and 7(a).

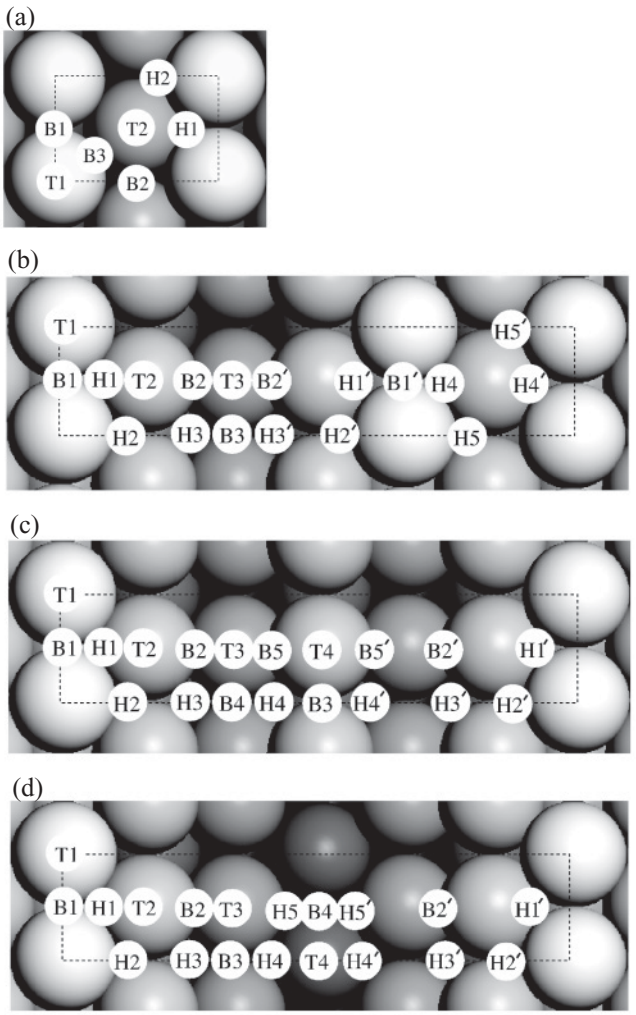

FIG. 4. Top views of (a) Re(10$\bar{1}$0)-(1 × 1), (b) Re(10$\bar{1}$0)-(1 × 3) single-MR, (c) Re(10$\bar{1}$0)-(1 × 3) double-MR, and (d) Re(10$\bar{1}$0)-(1 × 3) triple-MR surfaces, showing all binding sites at which O adsorption has been studied. The Re(10$\bar{1}$0)-(1 × 3) single-MR surface can be viewed as a combination of the unreconstructed Re(1010)-(1 × 1) and the reconstructed Re(1010)-(1 × 2) surfaces (not shown here).

(*a*) *Unreconstructed O/Re(10*$\bar{1}$*1)-(1 × 1).* For (2 × 2)-1O overlayers with $\Theta = 0.25$ GML, the threefold hollow H1 site is energetically preferred with $E_{\text{bind}} = 3.79$ eV [see Fig. 6(b)].

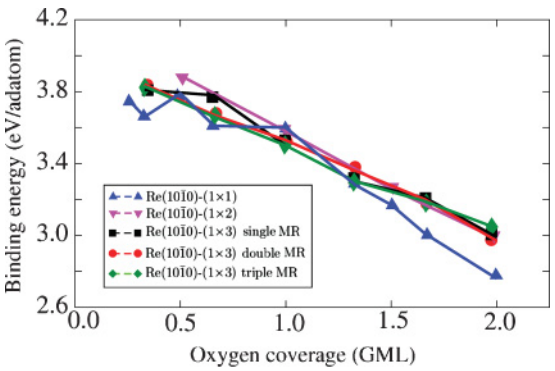

FIG. 5. (Color online) Binding energy (referenced to 1/2 O_2) as a function of oxygen coverage on Re(10$\bar{1}$0).

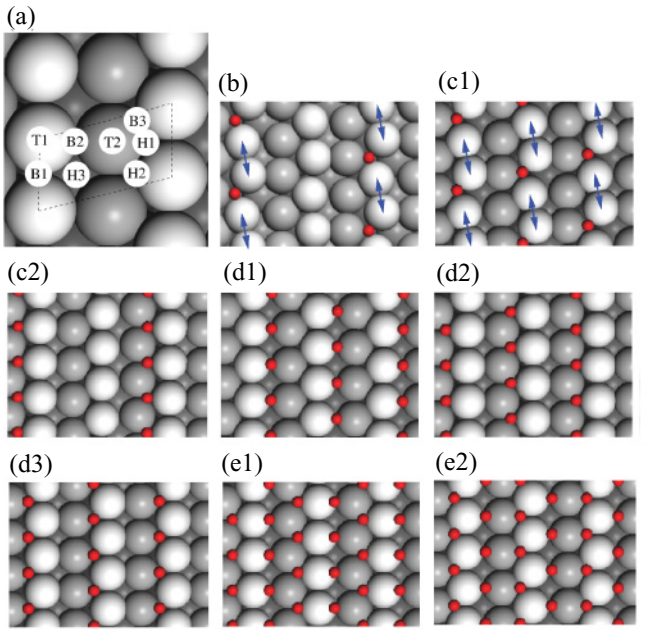

FIG. 6. (Color online) Top views of (a) Re(10$\bar{1}$1)-(1 × 1), showing all binding sites at which O adsorption has been studied, and the most stable structures of oxygen-covered unreconstructed Re(10$\bar{1}$1): (b) (2 × 2)-1O at 0.25 GML, (c1) (2 × 1)-1O and (c2) (1 × 2)-1O at 0.50 GML, (d1)–(d3) (1 × 1)-1O at 1.00 GML, and (e1) and (e2) (1 × 1)-2O at 2.00 GML. The arrows indicate the Re atoms that move toward each other upon relaxation (row pairing).

For 0.5 GML we focused on the (2 × 1)- and (1 × 2)-1O adlayers and found the former structure to be more stable. In this configuration oxygen again binds most strongly at the H1 site [Fig. 6(c1)] for which we calculated a binding energy of 3.80 eV. On the basis of the adsorbate distances, we expect that O–O repulsion has no significant contribution to the adsorption energy at H1 sites for (2 × 1)-1O (0.50 GML) and (2 × 2)-1O (0.25 GML) adlayers. Therefore, the RP effect can be a determining factor in influencing the overall adsorption. Since the number of row-paired atoms is the same for 0.50 and 0.25 GML, the calculated E_{bind} values in these two cases are very similar.

In the (1 × 2)-1O overlayer, RP is absent on the surface (for all studied adsorption sites) due to geometrical constraints. Interestingly, now the H2 site [Fig. 6(c2)] becomes most stable ($E_{\text{bind}} = 3.65$ eV). The (1 × 2)-1O structure, in which Re atoms of each second row are allowed to relax, might be the precursor of the (1 × 2)-MR reconstruction observed on Re(10$\bar{1}$1) (see next subsection).

Since RP is absent for $\Theta = 1.0$ GML [(1 × 1)-1O adlayer], the binding energy is determined by the strength of O–Re and O–O interactions. In this case, the binding oxygen at the B2, H2, and H1 sites [see Figs. 6(d1)–6(d3)] is the highest among all the considered sites.

Using the position labeling of Fig. 6(a), five possible combinations of distinguishable surface sites have been studied at 2.0 GML. We found that a structure in which O atoms occupy the first and second favorable sites (found at 1.0 GML), B2 and H2, has the highest overall binding energy of 3.11 eV [see Fig. 6(e1)], while a structure with adsorbed O at the first (B2)

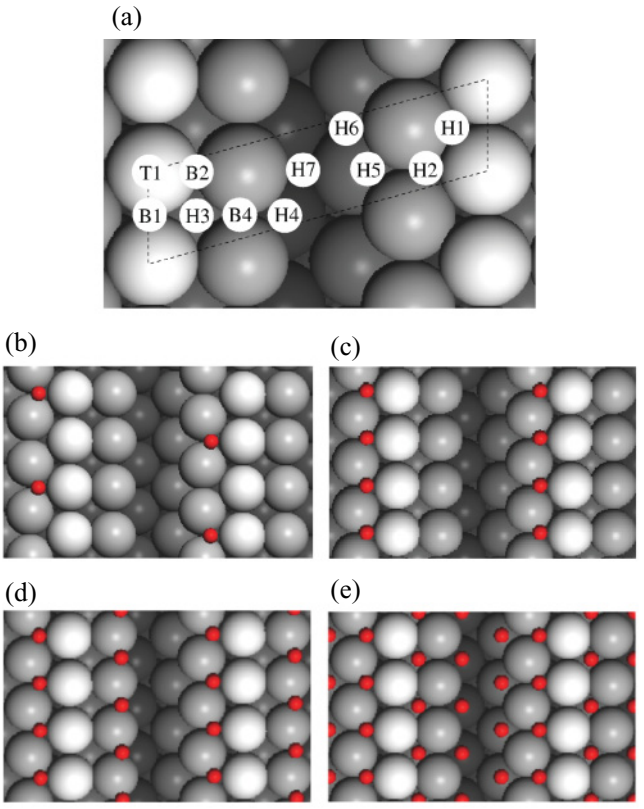

FIG. 7. (Color online) Top views of (a) Re(10$\bar{1}$1)-(1 × 2), showing all binding sites at which O adsorption has been studied, and the most stable structures of oxygen-covered reconstructed Re(10$\bar{1}$1)-(1 × 2): (b) (2 × 1)-1O at 0.25 GML, (c) (1 × 1)-1O at 0.50 GML, (d) (1 × 1)-2O at 1.0 GML, and (e) (1 × 1)-4O at 2.0 GML.

and third (H1) favorable sites [see Fig. 6(e2)] is only 0.01 meV less stable.

(*b*) *Reconstructed O/Re(10$\bar{1}$1)-(1 × 2)*. At Θ = 0.25 GML (in a (2 × 1)-1O adlayer), we found that the threefold H2 site [Fig. 7(b)] is the preferred position. For one O per unit cell (Θ = 0.50 GML in a (1 × 1)-1O structure), this site is still the most stable position for O. The calculated binding energy for this case is 0.03 eV lower than with Θ = 0.25 GML. Since the row pairing of the Re atoms in the topmost surface layer of (2 × 1)-1O was found to be negligible, the reduction in binding energy is related to a weak lateral O–O repulsion along the closely packed rows.

The binding energy at the H2 site in the (1 × 1)-1O adlayer on Re(10$\bar{1}$1)-(1 × 2) is 0.22 eV larger than that in the same overlayer on unreconstructed Re(10$\bar{1}$1)-(1 × 1). This suggests that removing every second row of topmost Re atoms has a significant effect on the oxygen binding energy at this site. This is also in line with our results for O atoms at H2 sites on the unreconstructed surface. There we found that the (1 × 2)-1O adlayer, in which binding to every second rows is absent, is more favorable than the (2 × 1)-1O overlayer.

Regarding 1.0 GML, among the studied systems we find the structure with oxygen atoms at H2 and B4 sites [see Fig. 7(d)] to be the most stable, giving a binding energy of 3.60 eV. The corresponding $\bar{E}_{\text{bind}}$ value is only 0.02 eV larger, which

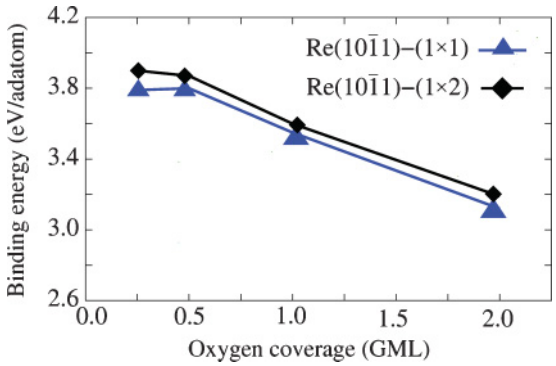

FIG. 8. (Color online) Binding energy (referenced to 1/2 O_2) as function of the oxygen coverage on Re(10$\bar{1}$1)-(1 × 1) and Re(10$\bar{1}$1)-(1 × 2).

shows that both oxygen atoms behave as almost independent adsorbates at this coverage.

Finally, the preferred structure at Θ = 2.0 GML [Fig. 7(e)] with an adsorption energy of 3.19 eV and $\bar{E}_{\text{bind}}$ = 3.52 eV shows much stronger interactions between adatoms compared to the lower-coverage systems (Θ = 0.5 and 1 GML). The change in binding energy upon increasing the oxygen coverage on Re(10$\bar{1}$1)-(1 × 1) and Re(10$\bar{1}$1)-(1 × 2) is summarized in Fig. 8. Our calculations show the influence of removing entire atomic rows (going from the unreconstructed to the (1 × 2)-reconstructed surfaces): The adsorption energy of oxygen atoms on the reconstructed structure is higher for all coverages. This preference remains almost constant between 0.25 and 2.00 GML. Therefore, our calculations qualitatively support the experimental observation of a (1 × 2) reconstruction on the O-covered {10$\bar{1}$1} faces. However, for a quantitative comparison of the stabilities of these structures we have to compare their surface free energies (see Sec. III C).

4. O/Re(11$\bar{2}$1)

Re(11$\bar{2}$1) is the substrate orientation onto which faceting occurs after adsorption of strongly interacting adsorbates (i.e., oxygen or nitrogen).[15] Figure 9(a) shows 13 probable binding sites that were considered in the present work. For coverages of 0.5 [(1 × 2)-1O and (2 × 1)-1O overlayers] and 1.0 GML [(1 × 1)-1O overlayer], oxygen prefers binding at twofold bridge sites (B5) (see Fig. 9). The calculated binding energies for these structures (Table II) are very similar. This is due to the following reasons: (i) Re(11$\bar{2}$1) is a rather open surface, and there are only weak adatom–adatom interactions in these overlayers, and (ii) the energy gain due to RP (the Re atoms of the first and second layers form zigzag rows) is negligible at 0.5 GML. Contrary to expectation, the strength of O–Re interactions (i.e., oxygen binding energy for the lowest studied coverage) on this high-index surface is not considerably stronger than on close-packed Re(10$\bar{1}$0) and Re(10$\bar{1}$1).

At 3.0 GML, as a consequence of repulsive interactions between adsorbates, the third added O atom per unit cell moves into the H3 position that was an unstable binding site at 1.0 GML. The binding energy curve of O/Re(11$\bar{2}$1) as function of O coverage (Fig. 10) shows a linear decrease of E_{bind} for 1.0 GML ⩽ Θ ⩽ 3.0 GML due to O–O interactions.

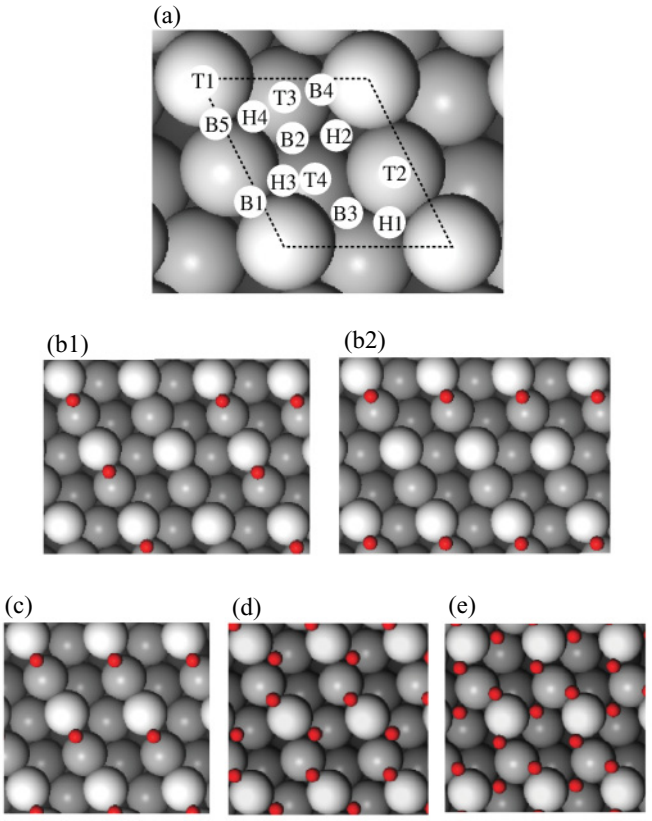

FIG. 9. (Color online) Top views of (a) Re(11$\bar{2}$1), showing all binding sites at which O adsorption has been studied, as well as the most stable structures of oxygen-covered Re(11$\bar{2}$1) with different overlayers and coverages: (b1) (1 × 2)-1O and (b2) (2 × 1)-1O at 0.5 GML, (c) (1 × 1)-1O at 1.0 GML, (d) (1 × 1)-2O at 2.0 GML, and (e) (1 × 1)-3O at 3.0 GML.

5. O/Re(13$\bar{4}$2)

Experimentally, it was found that nitrogen adsorption causes the Re(11$\bar{2}$1) surface to become completely faceted, forming two-sided ridgelike structures.[13] The orientations of the faces of the ridges are (13$\bar{4}$2) and (31$\bar{4}$2), which are surprisingly much more open compared to the initial Re(11$\bar{2}$1) surface. As reported in Ref. 37, our theoretical investigations showed that from a thermodynamical point of view N/Re(13$\bar{4}$2) is significantly more stable than N/Re(11$\bar{2}$1).

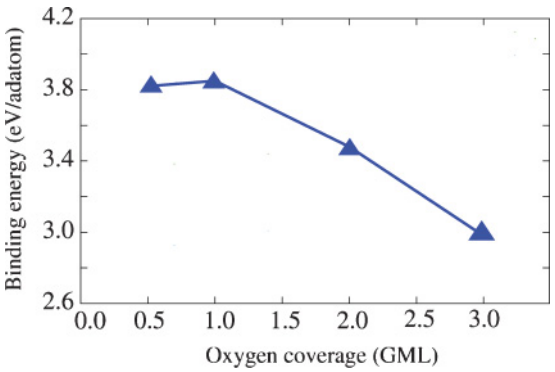

FIG. 10. (Color online) Binding energy (referenced to 1/2 O_2) as function of oxygen coverage on Re(11$\bar{2}$1).

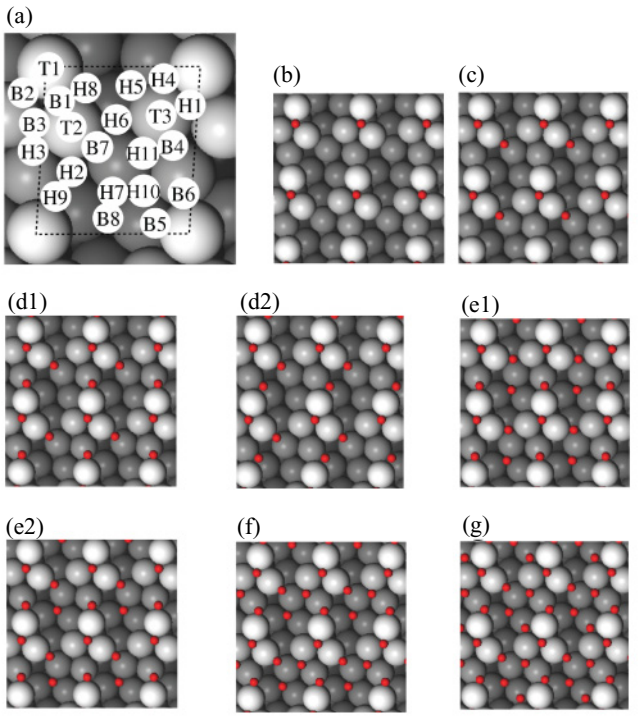

FIG. 11. (Color online) Top views of (a) Re(13$\bar{4}$2), showing all binding sites at which O adsorption has been studied, as well as the most stable structures of oxygen-covered Re(13$\bar{4}$2) with different overlayers and coverages: (b) (1 × 1)-1O at 1.0 GML, (c) (1 × 1)-2O at 2.0 GML, (d1) and (d2) (1 × 1)-3O at 3.0 GML, (e1) and (e2) (1 × 1)-4O at 4.0 GML, (f) (1 × 1)-5O at 5.0 GML, and (g) (1 × 1)-6O at 6.0 GML.

Here we discuss the adsorption of atomic oxygen (for coverages ranging from 1.0 to 6.0 GML) on Re(13$\bar{4}$2), which has been found to have unique properties.[15,37]

This surface exhibits many different adsorption sites. Figure 11(a) shows 21 probable binding sites, which we assumed as initial positions for binding. The most stable binding site for 1.0 GML is a threefold hollow H1 site [Fig. 11(b)], where each adsorbate binds to first-, second-, and third-layer Re atoms, with a binding energy of 4.03 eV. This value is higher than that obtained at similar threefold hollow sites on Re(0001), Re(10$\bar{1}$0), and Re(10$\bar{1}$1) and also at the twofold bridge sites on Re(11$\bar{2}$1).

As a consequence of the large surface unit cell of Re(13$\bar{4}$2), we observe minor O–O repulsion for 2.0 GML $\leqslant \Theta \leqslant$ 4.0 GML. The calculated adsorption energies for the most stable structures at $\Theta = 2.0$ [Fig. 11(c)] and 3.0 GML [Figs. 11(d1) and 11(d2)] are 3.78 and 3.67 eV, which are both only 0.13 eV smaller than the corresponding $\bar{E}_{\mathrm{bind}}$ values [see Eq. (5)]. At a coverage of 4.0 GML, the favored configuration [Fig. 11(e1)] has a binding energy of 3.55 eV, which is 0.07 eV lower than the value obtained for $\bar{E}_{\mathrm{bind}}$. For this coverage, the second favorable structure, shown in Fig. 11(e2), is only 0.01 eV less stable than structure 11(e1).

A relatively strong O–O interaction between the adatoms is found for 5.0 and 6.0 GML. At 5.0 GML [Fig. 11(f)], the fifth O atom binds at the vacant H11 position on the second favorable configuration we had obtained for 4.0 GML

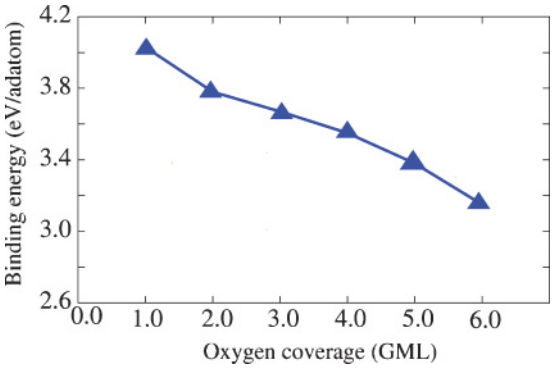

FIG. 12. (Color online) Binding energy (referenced to $1/2\ O_2$) as a function of oxygen coverage on Re(13$\bar{4}$2).

[Fig. 11(e2)], and the binding site of one of the preadsorbed atoms changes from H6 to B7 during geometry optimization (to minimize adsorbate–adsorbate repulsions). The relatively strong O–O interaction between adatoms is also confirmed by the calculated binding energy of 3.38 eV, which is 0.21 eV lower than the corresponding $\bar{E}_{\text{bind}}$ value.

From Fig. 12 it can be clearly seen that the binding energy decreases with increasing O coverage. Since, as mentioned, there is only weak O–O repulsion for 2.0 GML $\leqslant \Theta \leqslant$ 4.0 GML, the reduction in binding energy for the low coverages is mainly due to the energy differences between different occupied sites. Furthermore, the drop in the adsorption energy is not as strong as compared to that observed on Re(10$\bar{1}$0), Re(10$\bar{1}$1), and Re(11$\bar{2}$1).

C. Surface phase diagrams

The total energies obtained for the most favorable structures of the clean and O-covered Re surfaces have then been used to generate O/Re surface phase diagrams using Eq. (2). The resulting diagrams, where the surface free energies of different structures are plotted versus the chemical potential of the surrounding oxygen atmosphere, referenced by $\Delta\mu_O = \mu_O - \frac{1}{2}E^{\text{tot}}_{O_2}$, are shown in Fig. 13 for the various rhenium surfaces studied here. Since we are only interested in oxygen adsorption on pure Re surface, we shaded the oxygen chemical potential ranges ($\Delta\mu_O \geqslant -2.24$ eV) at which ReO_2 bulk oxide is the thermodynamically stable phase.[38] Of course, the presence of a stable surface oxide cannot be excluded and would certainly be of interest; however, we are not aware of any experimental study of surface oxide formation on the Re surfaces studied here. However, from our phase diagrams one might expect the formation of ReO_2 surfaces for oxygen chemical potentials higher than −2.24 eV. In order to illustrate the temperature and pressure dependence, the corresponding temperature scales for two different pressures are given above each diagram: 10^{-13} atm (comparable to UHV) and 1 atm (roughly ambient conditions).

1. O/Re(0001)

Figure 13 indicates that for oxygen chemical potentials below −3.55 eV oxygen completely desorbs from the surface. For −3.55 eV $\leqslant \Delta\mu_O \leqslant$ −3.22 eV, the (2 × 2)-2O overlayer with $\Theta = 0.50$ GML [Fig. 2(c)] proposed by Ducros *et al.*[4] and Zehner *et al.*[5] becomes stable. Although the (2 × 2) pattern might be due to the (2 × 2)-2O overlayers or even the (2 × 2)-1O adlayer [Fig. 2(b)] according to the LEED measurements reported in the latter study, our surface free energy plot makes apparent that the (2 × 2)-1O adlayer with $\Theta = 0.25$ GML does not appear as a stable phase at all. Therefore, in agreement with Ducros *et al.*[4] we expect that the observed (2 × 2) pattern should correspond to the (2 × 2)-2O structure with $\Theta = 0.50$ GML (phase *b*).

For −3.20 eV $\leqslant \Delta\mu_O \leqslant$ −2.24 eV, the (1 × 1)-1O structure that has been observed by Zehner *et al.*[5] for high coverages of O should form. Finally, from the thermodynamic viewpoint, increasing the oxygen chemical potential to and above −2.24 eV results in the formation of the ReO_2 bulk oxide.

2. O/Re(10$\bar{1}$0)

The O/Re(10$\bar{1}$0) phase diagram (Fig. 13) shows that for oxygen chemical potentials of $\Delta\mu_O <$ −3.67 eV desorption of oxygen should occur and clean unreconstructed Re(10$\bar{1}$0)-(1 × 1) is thermodynamically preferred over clean reconstructed Re(10$\bar{1}$0)-(1 × 2) or Re(10$\bar{1}$0)-(1 × 3) (see Fig. 4).

Increasing the oxygen chemical potential results in the formation of a c(2 × 4)-2O overlayer on unreconstructed Re(10$\bar{1}$0)-(1 × 1) between $\Delta\mu_O =$ −3.67 and −3.56 eV. Further increase up to −1.85 eV results in an increase of the adsorbate coverage on the unreconstructed surface (i.e., the (1 × 1)-1O, (1 × 3)-4O, and (1 × 2)-3O adlayers are formed, respectively).

Interestingly, for $\Delta\mu_O \geqslant$ −1.85 eV, a (1 × 3)-6O overlayer on the reconstructed Re(10$\bar{1}$0)-(1 × 3) triple-MR surface becomes the stable phase. The (1 × 3) reconstruction resembles a surface being composed of {10$\bar{1}$1} microfacets. This structure is able to rationalize the different experimental observations obtained on Re(10$\bar{1}$0). For further details we refer to Ref. 24.

3. O/Re(10$\bar{1}$1)

For $\Delta\mu_O \leqslant$ −3.80 eV, no oxygen is adsorbed on Re(10$\bar{1}$1), leading to a clean unreconstructed Re(10$\bar{1}$1)-(1 × 1) surface (see phase *a*). Since the oxygen binding energy on this surface is larger compared to other low-index Re(0001) and Re(10$\bar{1}$0) surfaces, adsorption of oxygen takes place at a lower value of $\Delta\mu_O$ (higher temperature at a fixed partial pressure) on Re(10$\bar{1}$1).

For −3.80 eV $\leqslant \Delta\mu_O \leqslant$ −2.70 eV the stabilized structures are the O-covered Re(10$\bar{1}$1)-(1 × 1) surfaces (phases *b* and *c*). For −2.70 eV $\leqslant \Delta\mu_O \leqslant$ −2.24 eV, there might be a coexistence of O-covered reconstructed Re(10$\bar{1}$1)-(1 × 2) and unreconstructed Re(10$\bar{1}$1)-(1 × 1) since their surface free energies are very similar. Only for high oxygen coverages of $\Theta \geqslant$2.0 GML does the surface become reconstructed.

This result is in agreement with experimental observations, showing a (1 × 2)-MR reconstruction on the (10$\bar{1}$1) faces in the presence of a large amounts of oxygen (exposures >100 L).[15]

4. O/Re(11$\bar{2}$1)

Oxygen desorption from this surface takes place above a chemical potential of −3.85 eV, which is lower than the corresponding values obtained for close-packed Re(0001),

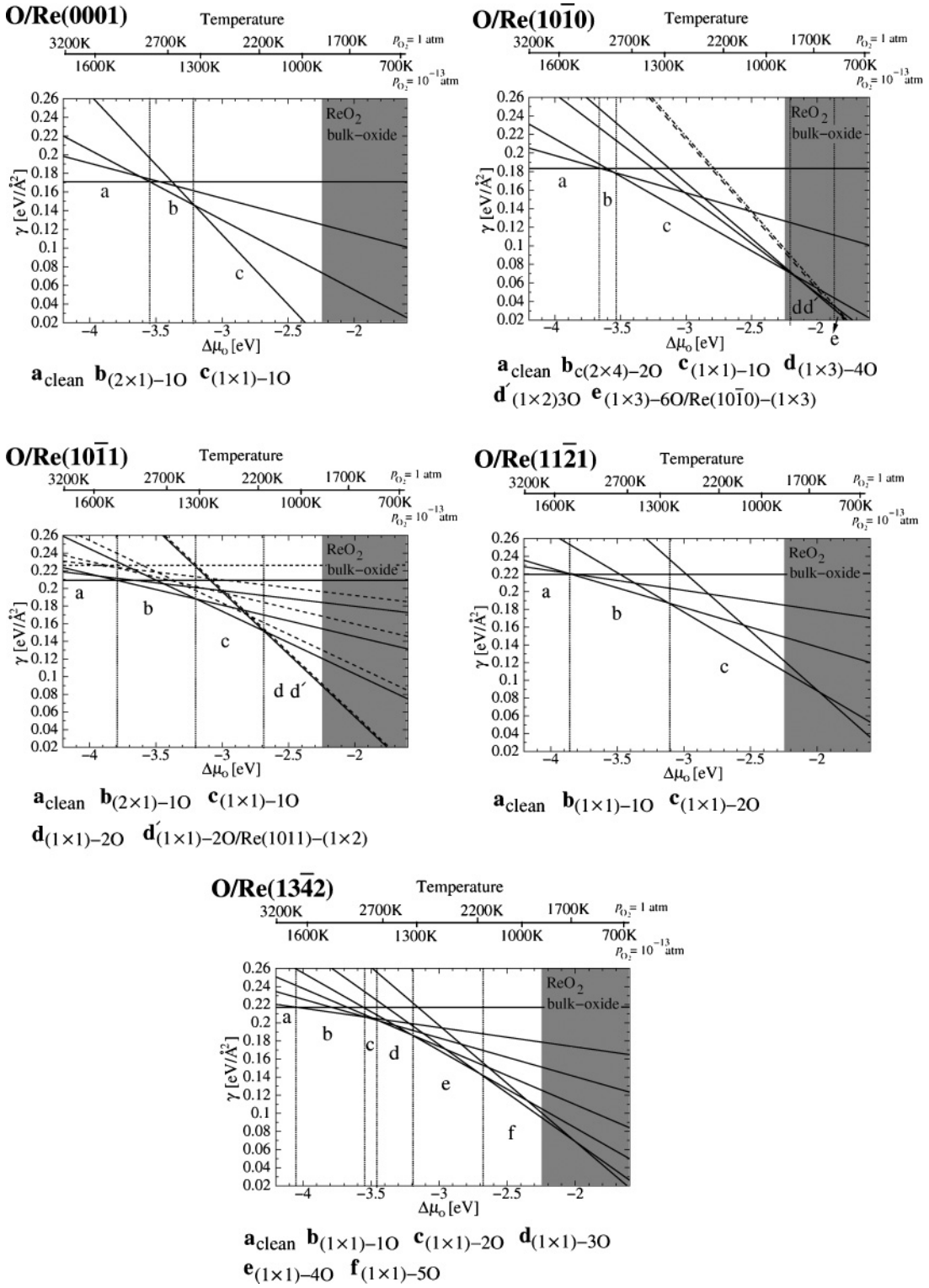

FIG. 13. Surface phase diagrams of O/Re surfaces showing the surface free energy as function of the oxygen chemical potential referenced as $\Delta\mu_O = \mu_O - \frac{1}{2}E^{tot}_{O_2}$. The most stable adlayer configurations on unreconstructed surfaces are labeled below each phase diagram, while reconstructions have been indicated in the label explicitly.

Re(10$\bar{1}$0), and Re(10$\bar{1}$1) surfaces. This is in agreement with the ordering of binding energies on these surfaces.

For -3.85 eV$\leqslant \Delta\mu_O \leqslant -3.10$ eV, the (1×1)-O adlayer ($\Theta = 1.0$ GML) becomes thermodynamically stable, while the (2×1)-O structure is not a stable phase at any value of $\Delta\mu_O$. If the RP effect was present, one would expect formation of this overlayer for very low values of oxygen chemical potentials ($\Delta\mu_O \sim -3.80$ eV), where the surface free energy of (2×1)-O is comparable to that of (1×1)-O, and a small energy gain similar to O/Re(0001) ($\sim$0.10 eV) would stabilize (2×1)-O.

Increasing $\Delta\mu_O$ above -3.10 eV causes the O coverage to increase to 2.0 GML. This structure is stable until the formation of the ReO_2 bulk oxide. Because of the strong destabilization arising from O–O repulsions, (1×1)-3O does not appear as a thermodynamically stable phase, although one might observe it as a metastable structure in the ReO_2 bulk oxide region.

5. *O/Re(13$\bar{4}$2)*

The critical oxygen chemical potential $\Delta\mu_O$, below which no oxygen adsorbs on the surface, is calculated to be -4.02 eV. This is the lowest value among the studied Re surfaces since the adsorption energy of O on Re(13$\bar{4}$2) is highest among the five surfaces (see Table II).

Above $\Delta\mu_O = -4.02$ eV, oxygen atoms start binding to the surface, while the oxygen coverage on Re(13$\bar{4}$2) increases gradually with $\Delta\mu_O$, finally reaching its maximum value of 5.0 GML before the ReO_2 bulk oxide should become thermodynamically stable.

IV. CONCLUSION AND OUTLOOK

We investigated clean and oxygen-covered surfaces of different Re orientations, from low to high Miller indices, considering different possible substrate and adsorbate configurations and coverages.

The determined stability of the clean surfaces, $\gamma_{0001} < \gamma_{10\bar{1}0} < \gamma_{10\bar{1}1} < \gamma_{13\bar{4}2} < \gamma_{11\bar{2}1}$, shows that it is not always the case that more open surfaces are less stable. The high-index Re(13$\bar{4}$2) surface possesses an unexpectedly high stability compared to Re(11$\bar{2}$1). This might be due to the fact that this surface can be viewed as Re(10$\bar{1}$1) terraces with steps and kinks.

On Re(0001), Re(10$\bar{1}$0), Re(10$\bar{1}$1), and Re(13$\bar{4}$2), oxygen prefers binding at the highly coordinated hollow sites, while on Re(11$\bar{2}$1) the twofold-coordinated bridge sites are favored. The comparison of binding energies calculated for the lowest oxygen coverages, where minor O–O repulsions can be expected, showed that the strength of O binding is highest at the most open surface, namely Re(13$\bar{4}$2), and weakest at the most close-packed surface, namely Re(0001). The adsorption energies on the other surfaces lie between these two limits: $E_{\text{bind}}^{0001} < E_{\text{bind}}^{10\bar{1}0} < E_{\text{bind}}^{10\bar{1}1} < E_{\text{bind}}^{11\bar{2}1} < E_{\text{bind}}^{13\bar{4}2}$.

On the basis of the binding energies for the most stable adlayer configurations we then generated corresponding surface phase diagrams. Comparing the different surfaces, we found that oxygen adsorption occurs at lower oxygen chemical potentials for more open surfaces, which is due to the stronger binding energy of O. Therefore, at fixed partial pressures, removal of oxygen atoms occurs at higher temperatures from higher-index surfaces.

Although clean Re(0001) is only 12 meV/Å^2 more stable than Re(10$\bar{1}$0), for very high oxygen coverages, prior to forming the ReO_2 bulk oxide ($\Delta\mu_O \sim -2.3$ eV), the former surface is more stable by 70 meV/Å^2. Under this condition, the surface free energy of Re(0001) is also considerably larger than even the values obtained for more open surfaces, namely Re(10$\bar{1}$1), Re(11$\bar{2}$1), and Re(13$\bar{4}$2).

In agreement with experimental studies we found that although clean Re(10$\bar{1}$0) and Re(10$\bar{1}$1) are unreconstructed, adsorption of atomic oxygen at high coverages ($\Theta \geqslant 2.00$ GML) might lead to (1×3)- and (1×2)-MR reconstructions, respectively. The former structure might form as a metastable phase, possibly stabilized due to kinetic limitations in the formation of ReO_2 bulk oxide, while the latter one is indeed thermodynamically stable.

Our work should have important implications for understanding the behavior and properties of Re-based oxidation catalysts that operate under oxygen-rich conditions since the catalysts' structures can dramatically affect their reactivity and selectivity for specific reactions. For instance, by a combined theoretical and experimental effort we could recently show that oxygen adsorption on Re(11$\bar{2}$1) below 1130 K leads to the formation of four-sided nanopyramids exhibiting Re(10$\bar{1}$0) and Re(01$\bar{1}$0) as well as (1×2)-reconstructed Re(10$\bar{1}$1) and Re(01$\bar{1}$1) faces.[15] Using different Re surfaces for investigating the structure sensitivity of catalytic oxidation reactions will be the next logical step.

Finally, by using the calculated surface free energies reported in the present work we have recently started to construct the equilibrium shapes of Re particles in the presence of oxygen and nitrogen, where we found drastic changes in the preferred particle shapes at high coverages. A comprehensive discussion of this effect will be the subject of a future presentation.

ACKNOWLEDGMENTS

The authors gratefully acknowledge support from the "Deutsche Forschungsgemeinschaft" (DFG) as well as from the bw-GRiD for computing resources.[39] Support from the European Union through the Marie-Curie Initial Training Network ELCAT, Proposal No. 214936-2, 2008-2012, is also acknowledged.

*timo.jacob@uni-ulm.de; http://www.echem.uni-ulm.de

[1] G. Wulff, Z. Kristallogr. **34**, 449 (1901).
[2] R. Ducros, M. Alnot, J. J. Ehrhardt, M. Houlsey, G. Piquard, and A. Cassuto, Surf. Sci. **94**, 154 (1980).
[3] R. Ducros, J. Fusy, J. Jupille, P. Pareja, and S. Tatarenko, Appl. Surf. Sci. **29**, 179 (1987).
[4] R. Ducros, M. Housley, and G. Piquard, Phys. Status Solidi **56**, 187 (1979).
[5] D. M. Zehner and H. E. Farnsworth, Surf. Sci. **30**, 335 (1972).
[6] H. P. Bonzel, D. K. Yu, and M. Scheffler, Appl. Phys. A **87**, 391 (2007).
[7] I. E. Wachs, G. Deo, A. Andreini, M. A. Vuurman, and M. de Boer, J. Catal. **160**, 322 (1996).
[8] Y. Z. Yuan, T. Shido, and Y. Iwasawa, Chem. Commun. **15**, 1421 (2000).
[9] J. Liu, E. Zhan, W. Cai, J. Li, and W. Shen, Catal. Lett. **120**, 274 (2008).
[10] M. E. Bussell, A. J. Gellman, and G. A. Somorjai, J. Catal. **110**, 423 (1988).

[11]M. Asscher, J. Carrazza, M. M. Khan, K. B. Lewis, and G. A. Somorjai, J. Catal. **98**, 277 (1986).
[12]R. Kojima, H. Enomoto, M. Muhler, and K. Aika, Appl. Catal. A-Gen. **246**, 311 (2003).
[13]H. Wang, Ph.D. thesis, Rutgers University, 2008.
[14]M. Reyhan, H. Wang, and T. E. Madey, Catal. Lett. **129**, 46 (2009).
[15]P. Kaghazchi, T. Jacob, H. Wang, W. Chen, and T. E. Madey, Phys. Rev. B **79**, 132107 (2009).
[16]E. Kaxiras, Y. Bar-Yam, J. D. Joannopoulos, and K. C. Pandey, Phys. Rev. B **35**, 9625 (1987).
[17]M. Scheffler, *Physics of Solid Surfaces* (Elsevier, Amsterdam, 1987).
[18]G.-X. Qian, R. M. Martin, and D. J. Chadi, Phys. Rev. B **38**, 7649 (1988).
[19]K. Reuter and M. Scheffler, Phys. Rev. B **65**, 035406 (2001).
[20]M. D. Segall, P. L. D. Lindan, M. J. Probert, C. J. Pickard, P. J. Hasnip, S. J. Clark, and M. C. Payne, J. Phys. Condens. Matter **14**, 2717 (2002).
[21]D. Vanderbilt, Phys. Rev. B **41**, 7892 (1990).
[22]J. P. Perdew, K. Burke, and M. Ernzerhof, Phys. Rev. Lett. **77**, 3865 (1996).
[23]P. Kaghazchi, Ph.D. thesis, Freie Universität Berlin, 2009.
[24]P. Kaghazchi and T. Jacob, Phys. Rev. B **81**, 075431 (2010).
[25]P. Kaghazchi and T. Jacob, Phys. Rev. B **76**, 245425 (2007).
[26]P. Kaghazchi, T. Jacob, I. Ermanoski, W. Chen, and T. E. Madey, ACS Nano **2**, 1280 (2008).
[27]D. R. Stull and H. Prophet, *JANAF Thermochemical Tables*, 2nd ed., edited by D. R. Stull and H. Prophet (US National Bureau of Standards, US EPO, Washinghton DC, 1971).
[28]H. L. Davis and D. M. Zehner, J. Vac. Sci. Technol. **17**, 190 (1980).
[29]D. Rosenthal, I. Zizak, N. Darowski, T. T. Magkoev, and K. Christmann, Surf. Sci. **600**, 2830 (2006).
[30]J. Lenz, P. Rech, K. Christmann, M. Neuber, C. Zubragel, and E. Schwarz, Surf. Sci. **270**, 410 (1992).
[31]T. R. Mattsson and A. E. Mattsson, Phys. Rev. B **66**, 214110 (2002).
[32]B. Hammer, L. B. Hansen, and J. K. Nørskov, Phys. Rev. B **59**, 7413 (1999).
[33]M. Gierer, H. Over, P. Rech, P. Schwarz, and K. Christmann, Surf. Sci. Lett. **370**, L201 (1997).
[34]S. Schwegmann, A. P. Seitsonen, V. De Renzi, H. Dietrich, H. Bludau, M. Gierer, H. Over, K. Jacobi, M. Scheffler, and G. Ertl, Phys. Rev. B **57**, 15487 (1998).
[35]C. Stampfl and M. Scheffler, Phys. Rev. B **54**, 2868 (1996).
[36]M. Lindroos, H. Pfnür, G. Held, and D. Menzel, Surf. Sci. **222**, 451 (1989).
[37]P. Kaghazchi and T. Jacob, Phys. Rev. B **82**, 165448 (2010).
[38]K. T. Jacob, S. Mishra, and Y. Waseda, Thermochim. Acta **348**, 61 (2000).
[39]bwGRiD (http://www.bw-grid.de) is a member of the German D-Grid initiative, funded by the Ministry for Education and Research (Bundesministerium für Bildung und Forschung) and the Ministry for Science, Research and Arts Baden-Württemberg (Ministerium fuer Wissenschaft, Forschung und Kunst Baden-Württemberg).